Microwave metamaterials made by fused deposition 3D printing of a highly conductive copper-based filament

Yangbo Xie, Shengrong Ye, Christopher Reyes, Pariya Sithikong, Bogdan-Ioan Popa, Benjamin J. Wiley, and Steven A. Cummer

Citation: Appl. Phys. Lett. 110, 181903 (2017); doi: 10.1063/1.4982718

View online: http://dx.doi.org/10.1063/1.4982718

View Table of Contents: http://aip.scitation.org/toc/apl/110/18

Published by the American Institute of Physics





Microwave metamaterials made by fused deposition 3D printing of a highly conductive copper-based filament

Yangbo Xie,^{1,a)} Shengrong Ye,^{2,a)} Christopher Reyes,² Pariya Sithikong,¹ Bogdan-Ioan Popa,³ Benjamin J. Wiley,^{2,b)} and Steven A. Cummer^{1,b)}

Department of Electrical and Computer Engineering, Duke University, Durham, North Carolina 27708, USA

²Department of Chemistry, Duke University, Durham, North Carolina 27708, USA ³Department of Mechanical Engineering, University of Michigan, Ann Arbor, Michigan 48109, USA

properties. Published by AIP Publishing. [http://dx.doi.org/10.1063/1.4982718]

This work reports a method for fabricating three-dimensional microwave metamaterials by fused deposition modeling 3D printing of a highly conductive polymer composite filament. The conductivity of such a filament is shown to be nearly equivalent to that of a perfect conductor for microwave metamaterial applications. The expanded degrees-of-freedom made available by 3D metamaterial designs are demonstrated by designing, fabricating, and testing a 3D-printed unit cell with a broadband permittivity as high as 14.4. The measured and simulated S-parameters agree well with a mean squared error smaller than 0.1. The presented method not only allows reliable and convenient fabrication of microwave metamaterials with high conductivity but also opens the door to exploiting the third dimension of the unit cell design space to achieve enhanced electromagnetic

Microwave metamaterials are engineered materials designed to interact with electromagnetic waves^{1–4} and exhibit useful effective material properties. Within the 0.3–3 GHz spectral range, such metamaterials are conventionally fabricated on printed circuit boards (PCBs).^{3,4} Conventional PCB-based fabrication of metamaterials, using methods such as chemical etching and computer numeric control (CNC) milling, limits the design space to two-dimensional planar structures and thus also restricts the performance of the metamaterials. Moreover, lossy PCB substrates such as FR-4 can cause substantial power absorption and further reduce metamaterial performance. The handling of toxic etchants (such as a ferric chloride solution) during chemical etching is often undesirable.

Some three-dimensional microwave metamaterials have been designed and realized, but most of these have been created by manually stacking the layers or arranging pieces of PCB-based planar metamaterials (a schematic is shown in Fig. 1(a).^{5–9} This manual stacking process is time-consuming and can suffer from inconsistent precision and assembly errors. More importantly, the metamaterial properties are still restricted by the inherent two-dimensional nature of the individual metamaterial structures in each layer of the stack.

Three-dimensional conducting metamaterial structures have been demonstrated by combining polymer 3D printing with metallization. One such method coats a polymer structure with metallic layers through methods such as thin film sputtering. ¹⁰ Another recently proposed alternative is to use the electroplating process to metallize the surface of a 3D printed structure. ^{11,12} While these methods circumvent many of the drawbacks of PCB-based fabrication approaches, there are disadvantages. Sputtering is a costly process, and both approaches require care to control the thickness of the

metallic layers. Unavoidable variability in this thickness creates uncertainty in the effective electromagnetic parameters.

In contrast, fully metallic additive manufacturing techniques are bringing about new opportunities for designing and fabricating novel 3D microwave metamaterials. Commercialized techniques are mostly laser-based, such as Direct Metal Laser Sintering (DMLS) and Selective Laser Melting (SLM). While these techniques can reliably produce strong structures with complex 3D geometries, they exhibit several disadvantages in fabricating microwave metamaterials: first, the fabrication facilities are expensive to own and maintain; second, the material (e.g., Titanium powder) and fabrication cost are also very high; ^{13,14} moreover, these techniques are generally limited to fabricate all-metal structures, without the flexibilities of integrating other materials (e.g., dielectrics).

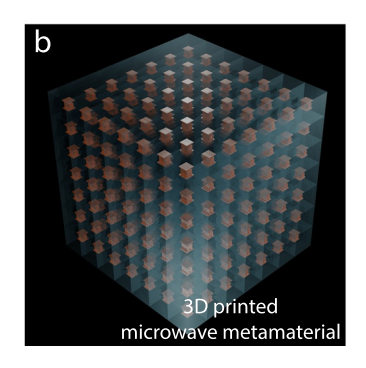
In this paper, we describe a method to fabricate threedimensional microwave metamaterials (we focus here in the frequency range of around 1 GHz) with Fused Deposition Modeling (FDM) 3D printing of a highly conductive filament (a schematic representation of the 3D printed microwave metamaterial is shown in Fig. 1(b). This recently introduced commercially available filament (trade named "Electrifi" 15) consists of a non-hazardous, proprietary metal-polymer composite that consists primarily of a biodegradable polyester and copper. The filament is compatible with most of the mainstream, relatively low-cost commercially available desktop 3D printers (such as Makerbot, LulzBot, and Prusa i-3 families), which is a significant advantage over other types of 3D metal printing methods in terms of accessibility and convenience. A picture of the printing process is shown in Fig. 1(c).

We will demonstrate below that although the conductivity of the filament $(1.67 \times 10^4 \, \text{S} \cdot \text{m}^{-1})$ is about 3600 times lower than that of copper, it is sufficiently high for microwave applications around 1 GHz.

⁽Received 8 February 2017; accepted 18 April 2017; published online 1 May 2017)

^{a)}Y. Xie and S. Ye contributed equally to this work

b) Authors to whom correspondence should be addressed. Electronic addresses: benjamin.wiley@duke.edu and cummer@ee.duke.edu



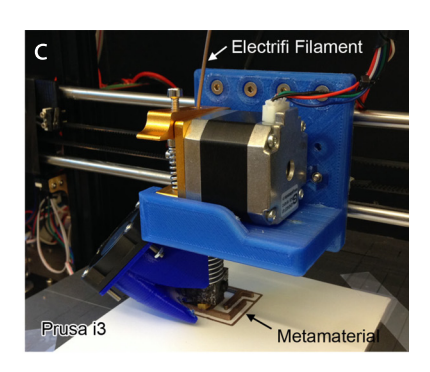


FIG. 1. Schematics of a conventional PCB-based metamaterial and a 3D printed metamaterial: (a) A metamaterial block made of stacked layers of conventional PCB-based unit cells, (b) a metamaterial block made of a periodic array of 3D-printed unit cells, and (c) FDM 3D printing of the highly conductive filament to create the 3D metamaterial.

The characterization of a material as "highly conductive" depends to a large extent on the operating frequency range. When driven by an electric field, a highly conductive material should allow unfettered electron flow through a "skin depth" layer, whose depth can be expressed as $\delta_{skin} = \sqrt{\frac{2}{\mu_0 \omega \sigma}}$, where the free space permeability $\mu_0 \approx 1.26 \times 10^{-6} \, H \cdot m^{-1}$. The skin depth, dependent on both the conductivity σ and the frequency ω , needs to satisfy $\frac{16}{\lambda_0} \frac{\delta_{skin}}{\lambda_0} = \frac{1}{\pi c_0} \sqrt{\frac{\omega}{2\mu_0 \sigma}} \ll 1$ so that in its dispersion relation $k^2 = \mu_0 \omega^2 \varepsilon + i \mu_0 \omega \sigma$, the imaginary part will dominate the right-hand-side. For example, a PCB with a 1/2 oz copper layer has a trace thickness of 18 microns, and its skin depth at 1 GHz is about 2 microns (assuming that the copper has a conductivity of $5.96 \times 10^7 \, \text{S/m}$), the value $\frac{\delta_{skin}}{\lambda_0} \approx 6.7 \times 10^{-6} \ll 1$, and thus, the copper trace can be regarded as a high conductivity structure around this frequency. However, the requirement

on the conductivity can be much less stringent as long as the value $\frac{\delta_{skin}}{\lambda_0}$ is two orders-of-magnitude smaller than unity (as confirmed with our numerical studies). For example, if we desire $\frac{\delta_{skin}}{\lambda_0} < 0.53\%$, a conductivity of more than $100\,\mathrm{S/m}$ would be sufficient.

We will first study the relationship between the effective material properties and the intrinsic material conductivity. It is intuitive that as conductivity approaches zero, the printed structures will behave as a dielectric, while as conductivity approaches infinity, the structure will behave as a perfect conductor. We present in Fig. 2 the numerical study of a unit cell (which we will study as an example in detail in later sections) that has a transition in permittivity when the conductivity is changed. At the left end of the axis of the conductivity (conductivity, $\sim 0.01 \, \text{S/m}$), the retrieved permittivity is close to unity, while at the right end (conductivity, $\sim 10^9 \, \text{S/m}$), the retrieved effective permittivity is close to a maximum of about 14.4. It is important to note that this high

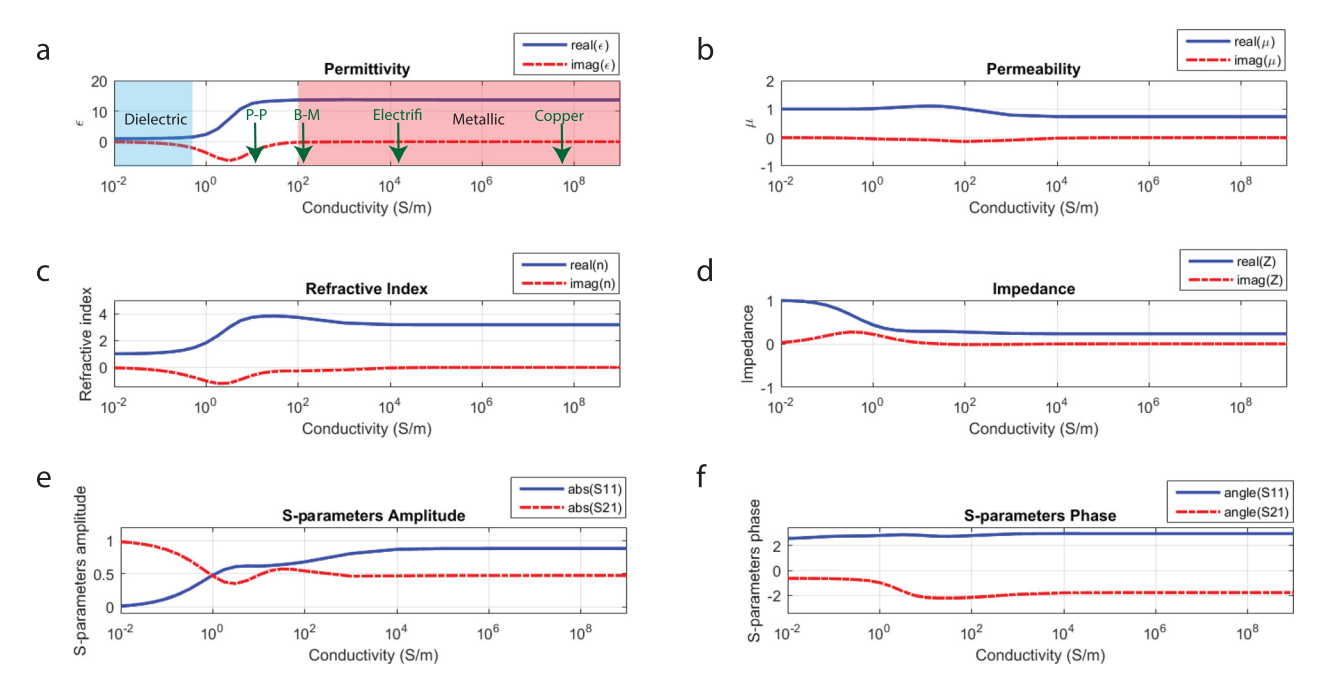


FIG. 2. The relationship between the conductivity and the effective material properties, obtained from full-wave simulations with a high permittivity metamaterial to be studied in detail in the later sections: (a) and (b) The permittivity and the permeability of the unit cell. In the permittivity plot, the high permittivity region on the right-hand side is highlighted in orange, and in this region, the filament behaves as a metal; the close-to-unity permittivity region on the left-hand side is highlighted in blue, and in this region, the filament behaves as a dielectric. The conductivity of copper, two commercially available conductive filaments Proto Pasta (P-P) and Black Magic (B-M), and the Electrifi filament used in our design and experiment are marked with green arrows. (c) and (d) The refractive index and the impedance of the unit cell. (e) and (f) The amplitude and phase of S-parameters of the unit cell.

effective permittivity remains relatively constant over several orders of magnitude of electric conductivity. As benchmarks, we annotate in Fig. 2(a) the conductivity of several materials: copper, the Electrifi conductive filament used in our experiment, and two other commercially available conductive filaments Proto Pasta and Black Magic. These results show that conductivity above roughly 10² S/m is required to achieve a strong and low-loss metamaterial response at 1 GHz.

The ability to conveniently and reliably 3D print using a sufficiently conductive filament provides extended degrees-of-freedom for metamaterial designs. Different from conventional PCB-based metamaterial designs that are restricted to planar structures and assembly, 3D designs can achieve larger charge storage surface areas, thicker current conducting channels, and complex 3D geometries to expand metamaterial responses to polarization and the angle of incidence. We demonstrate below a design example that exploits the extra spatial dimension to achieve enhanced broadband dielectric responses.

Dielectric metamaterial particles are desired for many wave controlling devices such as lenses⁷ and transformation optics-based devices. ^{17,18} One way to realize a strong dielectric response is to use resonant metamaterials to create an electric-field driven electric dipole response, e.g., with electric-field-coupled resonators. ¹⁹ However, if the broad bandwidth or low loss are desired, non-resonant broadband metamaterials are typically required. One of the typical broadband dielectric metamaterials is the so-called I-beam metamaterial, ¹⁷ which can be modeled as a series LC circuit. The electric permittivity originates from the capacitance of the structure, which generates an electrically driven electric dipole moment. The relationship between the effective permittivity and the local dipole moments in the unit cell can be expressed as

$$\varepsilon_{eff} = \frac{D}{\varepsilon_0 E_0} = 1 + \frac{P}{\varepsilon_0 E_0} = 1 + \frac{1}{\varepsilon_0 E_0 V_{uc}} \int_{V_{uc}} p(\vec{r}) d^3 \vec{r}, \quad (1)$$

where $p(\vec{r}) = \rho(\vec{r})(\vec{r_0} - \vec{r})$ is the local dipole moment and $(\vec{r_0} - \vec{r})$ is the displacement vector, and V_{uc} is the total volume of the unit cell.

In order to increase the value of the effective permittivity, we would like to increase the integral of the local dipole moment $p(\vec{r})$ in the volume of the unit cell. While the charge density $\rho(\vec{r})$ is roughly fixed for a given external electric field E_0 , according to Gauss's Law, the overall value of the integral can be effectively enhanced by engineering the local displacement vectors $(\vec{r_0} - \vec{r})$ (i.e., the geometry) of the structure. More specifically, a 3D unit cell designed with a larger effective surface area will create larger local dipole moments within the unit cell.

To verify this idea, we compare a conventional 2D dielectric metamaterial design with several 3D designs, as shown in Fig. 3. The 2D design we choose is a pair of parallel wires, which is a simplified I-beam unit cell with zero inductance (infinitely large resonant frequency). The extracted nonresonant permittivity is about 1.02, which, as expected, is not far from the value for vacuum. We then simply extrude the 2D design in the z-dimension to make a 3D unit cell: a pair of parallel plates. The extracted permittivity is about 1.17, 14.7% higher than the 2D version. To further enhance the dielectric responses, we borrow a technique that is used for designing a compact geometry with high capacitance, namely, coiling up the space to create more dipole moments. 9 Two 3D high dielectric unit cells (3D HD) are designed, and the numerical extraction shows high permittivity values of 4.79 and 14.44, respectively. The capacitance per unit cell of the four metamaterials is annotated next to their corresponding 3D models using a numerical method described in the supplementary material. This numerical study of the permittivity of the 3 types of 3D dielectric unit cells shows that significant enhancement of the dielectric response can be achieved by exploiting the design space in the third dimension. We also studied the influence of the geometrical parameters on the effective material properties of the 3D high-permittivity unit cell (see the supplementary material for details).

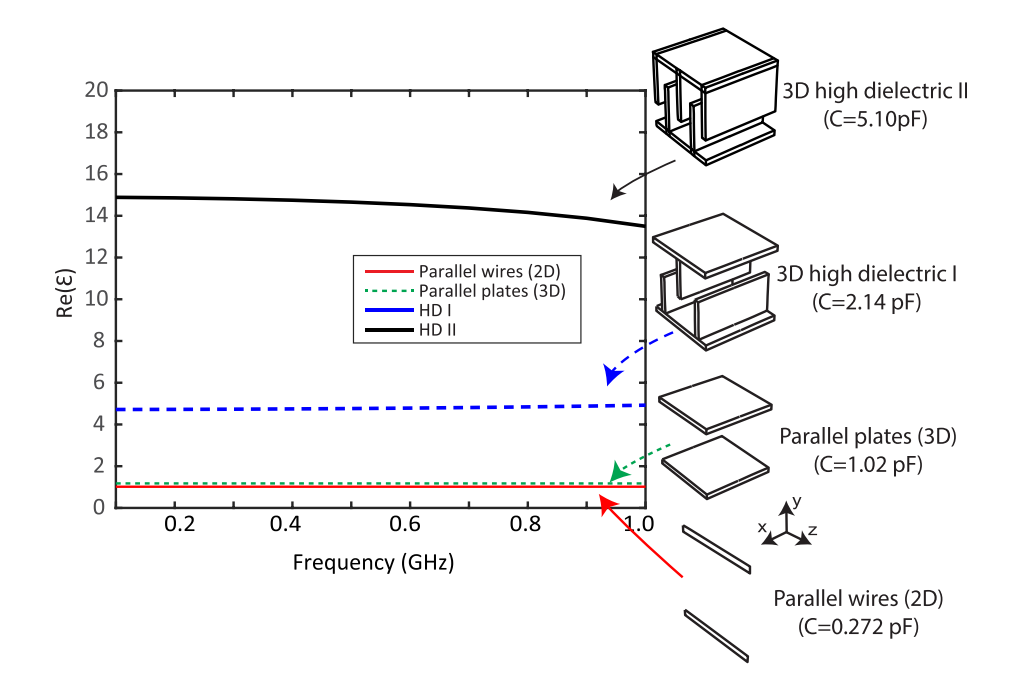


FIG. 3. The comparison of the permittivities of the 2D dielectric metamaterial and three different 3D dielectric metamaterials.

We experimentally verified the high dielectric responses of the 3D printed unit cells. A 3D model and a fabricated sample of the unit cell are shown in Figs. 4(a) and 4(b), respectively. Fig. 4(c) shows the setup of the numerical simulation, where a unit cell is placed in an ideal transverse electromagnetic (TEM) waveguide. The surface of the metamaterial is set to be a perfect electric conductor (PEC) to achieve the perfect conductivity. The boundary conditions of the simulated waveguide are set to the PEC condition on the top/bottom boundaries and to the perfect magnetic conductor (PMC) condition on the left/right boundaries so that a TEM mode can be formed in the frequency range of interest. In the experimental setup (Fig. 4(d)), 5 unit cells were arrayed in a microstrip waveguide that supports a TEM-like mode below the cutoff frequency of 5 GHz and mimics the retrieval setup in the simulation (Fig. 4(c)). A standard calibration and effective parameter retrieval method, 20,21 which includes a set of three measurements (empty waveguide, perfect reflector-loaded waveguide, and metamaterial-load waveguide), was used to eliminate errors introduced by the vector network analyzer and the transmission cables. The measured S-parameters were compared with the single unit cell retrieval simulation.

The measured S-parameters show excellent agreement (aside from a minor shift of the resonant frequency) with simulations across the entire $0.1-1.5\,\mathrm{GHz}$ frequency range. The mean squared error (MSE) between the measured data and the simulated data is only $0.0891\,\mathrm{for}\,\mathrm{S}11$ and $0.0799\,\mathrm{for}\,\mathrm{S}21$. The permittivity retrieved from the measurement has a non-negligible deviation from the expected value of around 1 GHz, even though the agreement is good for S-parameters. This is caused by the small value of the directly extracted impedance, and subsequently, the retrieved formula $\varepsilon = \frac{n}{Z}$ causes the amplification of the small deviation of S-parameters. This is also verified with evidence that the retrieved permittivity is much more sensitive to a small error of S11 than S21 (see the supplementary material for additional details). In the future, a retrieval method that

suppresses error amplification by proper regularization²² in the inverse problem would improve parameter retrieval for metamaterials with small impedances.

In conclusion, we presented in this paper a method of applying the FDM 3D printing technique to fabricate 3D gigahertz microwave metamaterials. The utilized FDM 3D printing technique is based on a high electrical conductivity filament with a conductivity of $1.67 \times 10^4 \, \text{S} \cdot m^{-1}$. We demonstrate with numerical simulations and measurements that the conductivity of the Electrifi filament can be useful for microwave engineering and specifically for designing and realizing microwave metamaterials.

The demonstrated 3D printing method not only allows reliable, convenient fabrication of metamaterials but also overcomes the restriction of the design space imposed by the conventional PCB-based 2D metamaterial design method. The third dimension can be effectively exploited to accommodate charge storage surface areas and current conducting structures to substantially enhance the electromagnetic response. A specific design example demonstrates how the 3D printing method can be used to facilitate the design and realization of a 3D metamaterial with high permittivity. Waveguide measurements were performed, and good agreement was found between numerical simulations and measurements.

This work opens the door to a variety of 3D metamaterial design opportunities. Besides designing 3D versions of the existing 2D unit cells (such as I-beams, electric-LC (ELC) resonators, and split-ring resonators (SRRs)) with enhanced material properties, unconventional designs may be explored to enrich the metamaterial unit cell library. Moreover, the controllable conductivity is an interesting feature that can be potentially explored to design functional devices such as efficient energy harvesters. We can expect in the near future that bulk metamaterials (as illustrated in Fig. 1(b)), consisting of a three-dimensional array of the 3D printed metamaterial unit cells as building blocks, can be manufactured automatically without the hassle and imprecision of manual assembly.

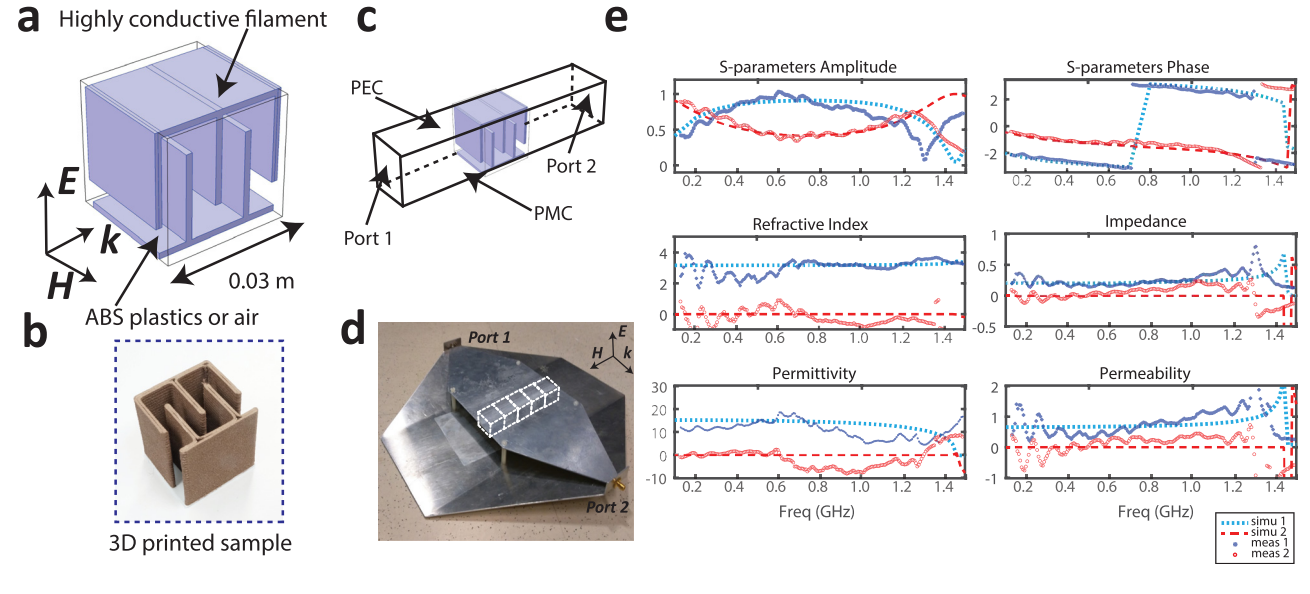


FIG. 4. The high permittivity metamaterial: (a) A 3D model of the unit cell, (b) a fabricated sample, (c) a microstrip waveguide measurement with 5 identical high permittivity metamaterials, (d) the simulation setup with a single high permittivity metamaterial in an ideal waveguide at the PEC condition on the top/bottom boundaries and the PMC condition on the left/right boundaries. The surface of the metamaterial is set to be PEC. (e) The comparison of the S-parameters and the retrieved refractive index/impedance and permittivity/permeability between the simulations and measurements.

See supplementary material for the description of the simulation method, the details about the employed highly conductive filament, and other related discussions.

This work was partially supported by the Multidisciplinary University Research Initiative grant from the Office of Naval Research (No. N00014–13-1–0631).

B.J.W. and S.Y. have an equity interest in Multi3D LLC, the manufacturer of Electrifi filament.

- ¹C. Caloz and T. Itoh, *Electromagnetic Metamaterials: Transmission Line Theory and Microwave Applications* (John Wiley & Sons, 2005).
- ²Metamaterials: Physics and Engineering Explorations, edited by N. Engheta and R. W. Ziolkowski (John Wiley & Sons, 2006).
- ³D. R. Smith, J. B. Pendry, and M. C. Wiltshire, "Metamaterials and negative refractive index," Science **305**(5685), 788–792 (2004).
- ⁴D. Schurig, J. J. Mock, B. J. Justice, S. A. Cummer, J. B. Pendry, A. F. Starr, and D. R. Smith, "Metamaterial electromagnetic cloak at microwave frequencies," Science **314**(5801), 977–980 (2006).
- ⁵M. Zedler, C. Caloz, and P. Russer, "A 3-D isotropic left-handed metamaterial based on the rotated transmission-line matrix (TLM) scheme," IEEE Trans. Microwave Theory Tech. **55**(12), 2930–2941 (2007).
- ⁶M. J. Freire, R. Marques, and L. Jelinek, "Experimental demonstration of a μ =-1 metamaterial lens for magnetic resonance imaging," Appl. Phys. Lett. **93**(23), 231108 (2008).
- ⁷N. Kundtz and D. R. Smith, "Extreme-angle broadband metamaterial lens," Nat. Mater **9**(2), 129–132 (2010).
- ⁸C. M. Soukoulis and M. Wegener, "Past achievements and future challenges in the development of three-dimensional photonic metamaterials," Nat. Photonics **5**(9), 523–530 (2011).

- ⁹Z. Liang, T. Feng, S. Lok, F. Liu, K. B. Ng, C. H. Chan, J. Wang, S. Han, S. Lee, and J. Li, "Space-coiling metamaterials with double negativity and conical dispersion," Sci. Rep. 3, 1614 (2013).
- ¹⁰I. M. Ehrenberg, S. E. Sarma, and B. I. Wu, "A three-dimensional self-supporting low loss microwave lens with a negative refractive index," J. Appl. Phys. 112(7), 073114 (2012).
- ¹¹S. M. Rudolph and A. Grbic, "A broadband three-dimensionally isotropic negative-refractive-index medium," IEEE Trans. Antennas. Propag. 60(8), 3661–3669 (2012).
- ¹²R. Zhu and D. Marks, "Rapid prototyping lightweight millimeter wave antenna and waveguide with copper plating," in 40th International Conference on Infrared, Millimeter, and Terahertz Waves (IRMMW-THz) (2015).
- ¹³I. Gibson, D. Rosen, and B. Stucker, Additive Manufacturing Technologies: 3D Printing, Rapid Prototyping, and Direct Digital Manufacturing (Springer, 2014).
- ¹⁴H. Lipson and M. Kurman, Fabricated: The New World of 3D Printing (John Wiley & Sons, 2013).
- 15 See https://www.multi3dllc.com (2017) for further information about Electrifi filament.
- ¹⁶R. Fitzpatrick, Maxwell's Equations and the Principles of Electromagnetism (Jones & Bartlett Publishers, 2008).
- ¹⁷R. Liu, C. Ji, J. Mock, J. Y. Chin, T. J. Cui, and D. R. Smith, "Broadband ground-plane cloak," Science **323**(5912), 366–369 (2009).
- ¹⁸H. Chen, C. T. Chan, and P. Sheng, "Transformation optics and meta-materials," Nat. Mater. 9(5), 387–396 (2010).
- ¹⁹D. Schurig, J. J. Mock, and D. R. Smith, "Electric-field-coupled resonators for negative permittivity metamaterials," Appl. Phys. Lett. 88(4), 041109 (2006).
- ²⁰X. Chen, T. M. Grzegorczyk, B. I. Wu, J. Pacheco, Jr., and J. A. Kong, "Robust method to retrieve the constitutive effective parameters of metamaterials," Phys. Rev. E 70(1), 016608 (2004).
- ²¹T. H. Hand, "Design and applications of frequency tunable and reconfigurable metamaterials," Doctoral dissertation (Duke University, 2009).
- ²²R. C. Aster, B. Borchers, and C. H. Thurber, *Parameter Estimation and Inverse Problems* (Elsevier Academic, 2005).